Received: 24 December 2022 | Revised: 25 February 2023 | Accepted: 13 March 2023

DOI: 10.1002/mp.16381

RESEARCH ARTICLE

MEDICAL PHYSICS

Towards fast adaptive replanning by constrained reoptimization for intra-fractional non-periodic motion during robotic SBRT

Stefan Gerlach[1] | **Theresa Hofmann**[2] | **Christoph Fürweger**[2] | **Alexander Schlaefer**[1]

[1]Institute of Medical Technology and Intelligent Systems, Hamburg University of Technology, Hamburg, Germany

[2]European Radiosurgery Center Munich, Munich, Germany

Correspondence
Stefan Gerlach, Institute of Medical Technology and Intelligent Systems, Hamburg University of Technology, Hamburg, 21073, Germany.
Email: stefan.gerlach@tuhh.de

Funding information
Deutsche Forschungsgemeinschaft, Grant/Award Numbers: SCHL 1844/3-2, SCHL 1844/6-1

Abstract

Background: Periodic and slow target motion is tracked by synchronous motion of the treatment beams in robotic stereotactic body radiation therapy (SBRT). However, spontaneous, non-periodic displacement or drift of the target may completely change the treatment geometry. Simple motion compensation is not sufficient to guarantee the best possible treatment, since relative motion between the target and organs at risk (OARs) can cause substantial deviations of dose in the OARs. This is especially evident when considering the temporally heterogeneous dose delivery by many focused beams which is typical for robotic SBRT. Instead, a reoptimization of the remaining treatment plan after a large target motion during the treatment could potentially reduce the actually delivered dose to OARs and improve target coverage. This reoptimization task, however, is challenging due to time constraints and limited human supervision.
Purpose: To study the detrimental effect of spontaneous target motion relative to surrounding OARs on the delivered dose distribution and to analyze how intra-fractional constrained replanning could improve motion compensated robotic SBRT of the prostate.
Methods: We solve the inverse planning problem by optimizing a linear program. When considering intra-fractional target motion resulting in a change of geometry, we adapt the linear program to account for the changed dose coefficients and delivered dose. We reduce the problem size by only reweighting beams from the reference treatment plan without motion. For evaluation we simulate target motion and compare our approach for intra-fractional replanning to the conventional compensation by synchronous beam motion. Results are generated retrospectively on data of 50 patients.
Results: Our results show that reoptimization can on average retain or improve coverage in case of target motion compared to the reference plan without motion. Compared to the conventional compensation, coverage is improved from 87.83 % to 94.81 % for large target motion. Our approach for reoptimization ensures fixed upper constraints on the dose even after motion, enabling safer intra-fraction adaption, compared to conventional motion compensation where overdosage in OARs can lead to 21.79 % higher maximum dose than planned. With an average reoptimization time of 6 s for 200 reoptimized beams our approach shows promising performance for intra-fractional application.
Conclusions: We show that intra-fractional constrained reoptimization for adaption to target motion can improve coverage compared to the conventional

approach of beam translation while ensuring that upper dose constraints on VOIs are not violated.

KEYWORDS
intra-fractional adaption, robotic radiation therapy, treatment planning

1 | INTRODUCTION

In robotic stereotactic body radiation therapy (SBRT),[1] the flexibility of a robotic arm allows for a steep dose gradient to spare healthy tissue and conformal treatment of the target. However, intra-fractional target motion, either due to breathing or spontaneous organ motion can influence the quality of the treatment. Automatic motion management by couch motion,[2] leaf motion of the multi-leaf collimator[3] or gating[4] can improve the accuracy of the delivered dose for conventional treatment devices. In clinical practice with the CyberKnife, treatment beams are moved synchronously to compensate target motion.[5] Compensation of small or periodic motion improves or enables dosimetric accuracy for many treatment sites.[6] In addition, 4D-planning accounting for the relative motion between beams and OARs has been studied for compensation of periodic motion.[7] However, large, non-periodic target motion which changes the geometric relationship between the target and surrounding organs at risk (OARs) can occur during treatment either by spontaneous events, for example, digestive flatulence, or target drift over time.[8,9] Crucially, this geometric change can significantly influence the delivered dose distribution and potentially lead to missing parts of clinical targets and increased toxicity in OARs.[8,9] Furthermore, margins could be reduced if more accurate treatment delivery is feasible. While translational or rotational compensation by beam motion for periodic motion can "wash out" dosimetric influence in surrounding OARs even if the target moves relative to the OARs, we show that large, non-periodic motion can be challenging for the conventional compensation method. A schematic illustration of the problem is shown in Figure 1.

We propose fast replanning of the treatment plan after target motion to improve treatment delivery after large intra-fractional target motion. So far, mostly inter-fractional replanning for intensity modulated radiation therapy (IMRT) has been studied. In particular, considering the clinical use of MR-Linacs, several inter-fractional replanning approaches have been proposed[10–12] which are often commercially available and can improve treatment delivery.[13] For many cases inter-fractional plan adaption is deemed beneficial.[14,15]

The problem of intra-fractional replanning poses several additional challenges. First, intra-fractional replanning is more time constrained since replanning has to be done during treatment after detection of a large target motion. Additionally, supervision for replanned treatment plans is also limited due to time constraints. Therefore, we argue that the ability to ensure hard constraints on the maximum dose in OARs is crucial to make replanning viable in clinical practice.

While fast treatment planning approaches have been explored,[16] only few approaches for intra-fraction replanning have been shown. Still, the potential benefits have been acknowledged.[17] One approach for intra-fractional replanning by Antico et al. is based on a library of simulated target motions to decide for the beam which promises the closest dose delivery compared to the prescribed dose distribution.[18] However, the treatment can be suboptimal due to deviations between the corresponding scenario in the library and the actual target motion as has been shown for inter-fractional replanning.[19] Furthermore, in robotic SBRT between 140 and 170 sequentially delivered treatment beams are typically involved,[20] compared to 5 to 9 fields that are commonly used in IMRT.[21] This greatly increases the combinatorial problem size for robotic SBRT, since target motion can occur at any time during the treatment, and makes generation of a library for every possible motion infeasible.

The approaches by Kontaxis et al. iteratively perform a fluence optimization and segmentation to find the best segment to deliver next without a complete segment weight optimization.[22–24] Similarly, Mejnertsen et al. show dose optimization with a simplified dose calculation algorithm for VMAT treatment.[25] However, the particular properties of robotic SBRT including the large number of beam angles make adaptation of these methods challenging. Additionally to the larger number of delivered beams, dose delivery in robotic SBRT is more heterogeneous over time. Due to the relatively small treatment fields in comparison to the target size and their quantity, every beam affects only a comparatively small volume but deposits high dose. Therefore, unfavorable target motion can lead to increases in OAR dose as is shown by Figure 2 where the same volume is reirradiated by a moved beam. With existing approaches for replanning and the conventional compensation by synchronous beam motion, no guarantees on the maximum dose can be provided.

We propose an approach including constrained optimization in the form of a linear program for replanning after large, non-periodic target motion for robotic motion compensated SBRT. Contrary to current approaches for intra-fractional replanning in IMRT, we ensure strict upper bounds on each voxel after replanning. Therefore, we avoid unexpected overdosage in OARs and normal

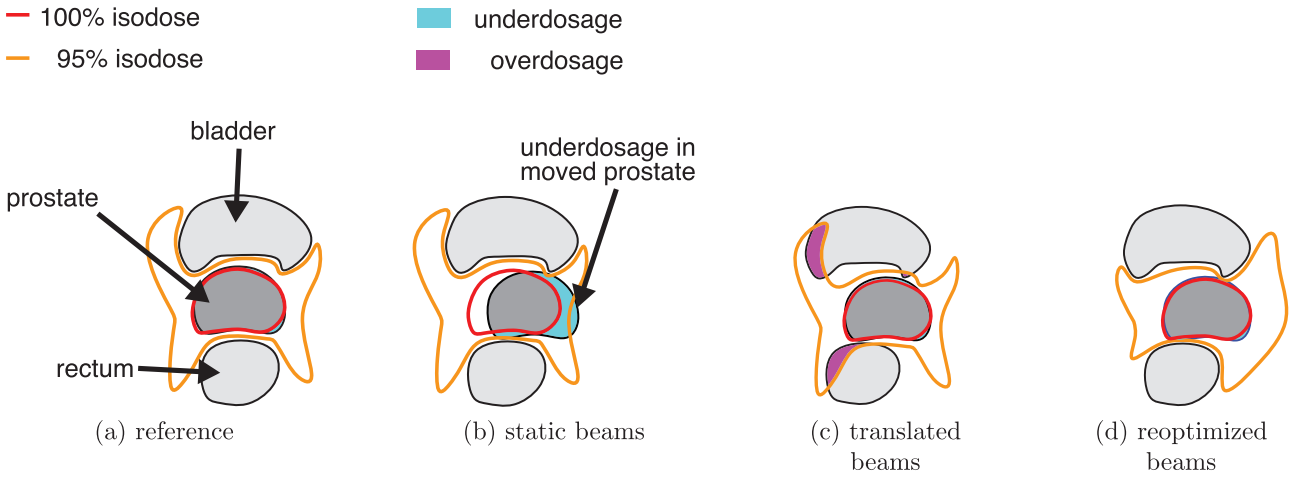

FIGURE 1 Illustration of dose distribution in the reference case without motion (a), with target motion but static beams (b), with synchronous beam motion (c), and with reoptimization of synchronously moved beams (d). Static beams can lead to underdosage in case of target motion, while synchronously moved beams can lead to overdosage in OARs which can be avoided using reoptimization. Note that isodoses are exaggerated to illustrate the effect. OARs, organs at risk.

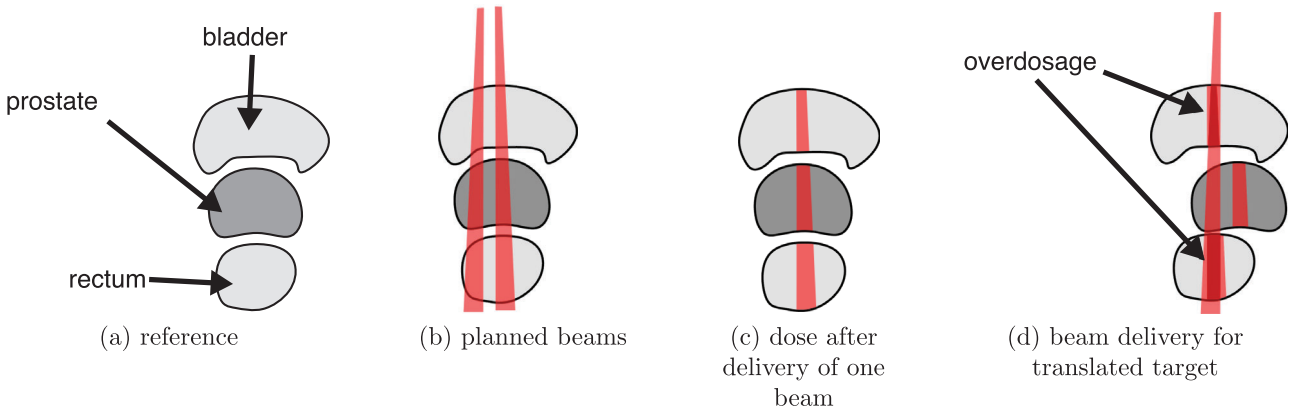

FIGURE 2 Illustration of overdosage due to heterogeneous dose delivery when target motion is compensated by the conventional approach of synchronous beam motion.

tissue to maintain a safe treatment. Our approach for replanning is fast (6 s) to be applicable in the clinical setting. We analyze our approach for 50 cases of patients who were previously treated for prostate cancer and multiple simulated motions in the range of clinically observed magnitudes. Our results show that replanning leads to improved actual delivered dose distribution when compared to the clinical practice of compensation by beam translation.

2 | METHODS

2.1 | Treatment planning for the static target

In this work we extend our inverse optimization approach for treatment planning.[26] We give a short overview of the planning pipeline here.

A treatment plan is generated based on CT data of the patient, where medical experts delineated the planning target volume (PTV) and relevant OARs. We define additional shell structures around the PTV at specific distances. During planning these shell structures control the dose gradient and dose in normal tissue.

Candidate beams with round collimators of different sizes[27] are then sampled based on a randomized heuristic. To ensure feasibility of plan delivery with the CyberKnife, beams can only be delivered from specific positions (beam nodes). We sample candidate beams by selection of a random beam node and target point on the projection of the PTV on a plane which is perpendicular to the line from beam node to PTV centroid (beam's eye view). Here, we weight points towards the border of the projection higher to improve coverage of the PTV.

Dose coefficients are then calculated for every beam and every voxel inside the volumes of interest (VOIs).

A dose coefficient for a beam and voxel $a_{b,v}$ describes the deposited dose of the beam into the voxel $d_{b,v}$ by $d_v = a_{b,v} \cdot w_b$. Here, w_b is the weight of the beam, that is, the beam-on time.

Upper dose constraints on PTV, OARs, and shell structures, prescribed dose to the PTV, and maximum monitor unit (MU) constraints are specified to conform with clinical goals. Finally, we formulate a linear optimization problem to solve for the optimal weighted subset of beams from the set of candidate beams. Here, the beam weight corresponds to the MU of the beam.

2.1.1 | Linear optimization for the inverse problem

The solution of the inverse planning problem identifies a weighted set of beams which is optimal regarding constraints, the candidate beam set, and the objective function. We indirectly optimize for coverage by minimizing underdosage in the PTV, solving

$$\min \sum_{v \in I_V} s_v \tag{1}$$

$$\text{s.t.} \quad A \cdot x - b_l + s \geq 0 \tag{2}$$

$$A \cdot x - b_u \leq 0 \tag{3}$$

$$\sum_{b \in I_B} x_b - m_u \leq 0 \tag{4}$$

$$x_b, s_v \geq 0 \quad \forall b \in I_B, \forall v \in I_V \tag{5}$$

Here, the matrix A contains dose coefficients $a_{b,v}$ for beam b affecting voxel v and the vector x contains the variable beam weights. x_b is an entry of the beam b in the vector x. I_B and I_V are the sets of all beams and voxels, respectively. b_u and b_l are the upper and lower dose constraints for OARs and PTV. The slack variables s_v in the vector s represent the underdosage in the PTV for each voxel v in the PTV and m_u is the constraint on the total MU.

We use a dual simplex based method implemented by IBM ILOG Cplex V20.1, IBM, NY to solve the optimization problem. Note that the solution is optimal with respect to the constraints. Furthermore, the constraints are strict and the solution does not exceed these constraints on the dose grid.

Commonly, beams with low MU after optimization are excluded from delivery since the error in delivered doses is larger for low MU beams and treatment time can thereby be reduced with little decrease in plan quality. Therefore, we remove beams with MU below $m_l = 6$ MU after optimization and reoptimize the weight of the remaining beams while adding an additional minimum MU constraint $x_b \geq m_l$ for all remaining beams.

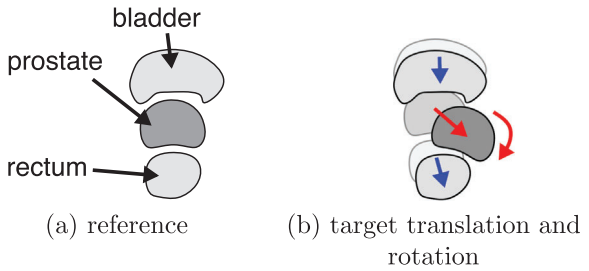

FIGURE 3 Illustration of the simulated target translation and rotation (b, red arrows) compared to the reference (a). OARs are translated if they would intersect with the target otherwise and non-overlapping OARs are moved to keep distances to the PTV similar compared to the reference (blue arrows). OARs, organs at risk; PVT, planning target volume.

2.2 | Simulation of target motion

In this study we intend to isolate the effect of replanning from tracking and assume perfect reconstruction of the actual target motion for replanning. To evaluate the effect of replanning alone, we assume that a large intra-fraction motion occurs once during the treatment between delivery of two beams, for example, due to sudden bowel movement.

To perturb the PTV pose, we apply a random translation and rotation. We sample a random direction vector and rotation vector from an isotropic distribution. For these vectors we then sample a magnitude and rotation angle from constrained normal distributions, respectively.

If the perturbed PTV overlaps with an OAR, we translate the OAR in the direction of a vector from perturbed PTV centroid to OAR centroid, until perturbed PTV and OAR do not overlap as Figure 3 shows. Additionally, we move the non-overlapping OAR towards the centroid of the original PTV to ensure that distances between PTV and OARs remain similar and to simulate a more natural change of VOI positions.

2.3 | Replanning

For replanning we optimize the inverse planning problem again between delivery of two beams by following the steps shown in Figure 4. Optimization speed and maintaining constraints are important to allow for intra-fraction replanning. To address optimization speed we limit the problem size and only consider weighted beams from the original plan as candidate beams to reweight those during replanning. Furthermore, we assume that the beams are translated and rotated synchronously with the target as is current clinical practice. Additionally, we move the artificial shell structures synchronously to the PTV motion.

To construct the replanning optimization problem, we adjust all upper (b_u) and lower (b_l) dose constraints and

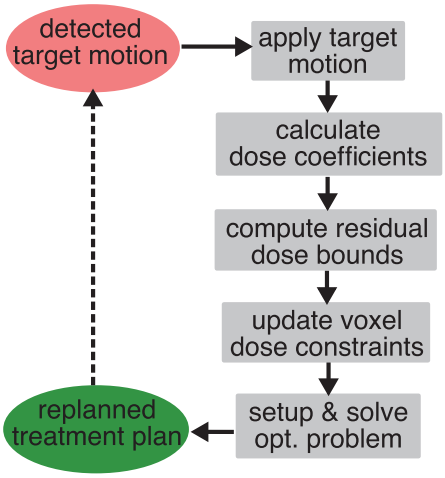

FIGURE 4 Flowchart of our proposed approach for replanning. Note that the detection of target motion is not further described in this work.

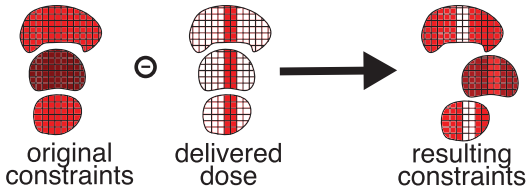

FIGURE 5 Illustration of constraint adaption. Delivered dose in the static geometry is mapped to the translated geometry. New constraints are derived by subtracting delivered dose from upper and lower dose constraints. Dark read means higher dose constraints.

additionally we adjust MU constraints m_u by the dose which is delivered before the target motion by

$$b_{u,\text{new}} = b_u - A_d \cdot x_d \tag{6}$$

$$b_{l,\text{new}} = b_l - A_d \cdot x_d \tag{7}$$

$$m_{u,\text{new}} = m_u - \sum_{b \in I_d} x_b \tag{8}$$

Here, A_d is the matrix of dose coefficients of beams delivered for the reference case, x_d are the weights of delivered beams, and I_d is the set of delivered beams. Essentially, we map the dose that is delivered before target motion to the perturbed patient geometry and subtract it from the original dose constraints as shown in Figure 5. Since the optimization problem is only evaluated in the VOIs, we map dose in each voxel of each VOI before target motion to the same voxel of the translated and rotated VOI.

The new matrix of dose coefficients A_{new} is calculated for the beams of the original treatment plan which have not yet been delivered. In this study, we do not consider changes of the CT due to target motion but in essence move the position of the voxels to calculate

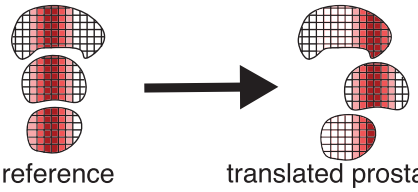

FIGURE 6 Coefficient calculation for beams after target motion. Shown are the coefficients for a single beam for reference and the resulting coefficients after the beam follows the target motion. Higher dose coefficients correspond to darker shades of red.

dose coefficients. As shown in Figure 6, the coefficients in the PTV are similar before and after PTV motion for small rotations but coefficients in the OARs can show large differences.

Finally, we set up the optimization problem for replanning by

$$\min \sum_{v \in I_V} s_v \tag{9}$$

$$\text{s.t.} \quad A_{\text{new}} \cdot x_r - b_{l,\text{new}} + s \geq 0 \tag{10}$$

$$A_{\text{new}} \cdot x_r - b_{u,\text{new}} \leq 0 \tag{11}$$

$$\sum_{b \in I_{r,B}} x_{r,b} - m_{u,\text{new}} \leq 0 \tag{12}$$

$$x_{r,b}, s_v \geq 0 \quad \forall b \in I_{r,B}, \forall v \in I_V \tag{13}$$

where x_r is the vector of beam weights $x_{r,b}$ of remaining beams. Note, that the specified constraints are guaranteed to not be exceeded by the resulting beam weights.

2.4 | Experimental setup

We retrospectively evaluate our approach for 50 patients previously treated for prostate cancer. For comparable results, we follow a simple protocol. We plan for 36.25 Gy prescribed dose to the PTV (prostate), 34 Gy upper dose constraints in the OARs (bladder and rectum), and 40.5 Gy upper dose constraint in the PTV. Additionally, we introduce shells around the PTV at 3 and 9 mm distance to control dose in normal tissue. Shell constraints are set such that 95% coverage is achieved for every patient for the reference case by automatic search. We use a 3×3 mm resolution for dose evaluation and optimization and generate beams with circular collimators of sizes 10 , 15, 20, 30, and 40 mm.

Note that the optimization results in an optimal weighted beam set which is typically a small subset of the candidate beam set. However, different candidate beam sets commonly produce different weighted beam sets. Therefore, we evaluate each case with 10 different candidate beam sets to increase statistical robustness.

TABLE 1 Values for the normal distributions which we use to sample magnitudes for simulated translation and rotation of the target. SD is standard deviation.

Mean	Minimum	Maximum	SD
2.5 mm	0 mm	5 mm	1 mm
7.5 mm	5 mm	10 mm	2 mm
12.5 mm	10 mm	15 mm	2 mm
1.75°	1°	2.5°	0.5°
3.5°	2°	5°	1°
7°	4°	10°	2°

The beams are usually delivered in a specific order such that the treatment time is minimal. Beams with short distance between their beam nodes are typically delivered within a short amount of time. We therefore approximate the clinical beam order by sorting the beams by the location of their beam node. We compare this sorted beam set to a randomly ordered beam set which may offer more homogeneous dose delivery over time.

We study motions in the range of previously reported findings[12,28–30] of up to 15 mm and 10° and sample 10 different translations and 10 different rotations for each case. Values are sampled from constrained normal distributions with mean, min, and max values and standard deviation shown in Table 1. We report significance according to the student's *t*-test with *p*-values smaller than 0.01.

3 | RESULTS

3.1 | Replanning considering translation

We evaluate the effect of motion adaption approaches on the treatment plan quality retrospectively for 50 patients. Figure 7 compares the resulting coverage of the treatment plan for the reference plan without target motion, with target motion but no compensation (static beams), with only translational compensation, and with reoptimization. Here, only target translation is simulated. When the mean translation of the PTV increases, the mean coverage decreases with static beams and translational compensation to 59.82% and 87.82% for mean translation of 12.5 mm, respectively ($p < 2.2e^{-16}$). Mean coverage for the reoptimized plans does not decrease below 94.81% compared to the reference case with a mean coverage of 94.85%. Difference in coverage between reference and reoptimized plans is not significant for 2.5 mm mean translation ($p = 0.0136$) but is significant for larger mean translations ($p < 0.00468$).

Furthermore, as shown in Figure 8, translational compensation results in up to 21.79% higher maximum dose than planned in the OARs. This overdosage is avoided with reoptimization.

Figure 9 shows the described effects for several cases. Additionally, Figure 10 shows the resulting dose contours for one case. In 73.49% of cases with 12.5 mm mean translation, at least one maximum dose constraint of the OARs was violated when using translated beams for compensation.

3.2 | Replanning considering rotation

When isolating the effect of rotation of the PTV, the average coverage decreases for static beams and rotational compensation to 92.81% and 94.14% for 7° mean rotation ($p < 2.2e^{-16}$), respectively, as shown in Figure 11. Average coverage is generally higher for reoptimized plans with rotation compensated beams and increases slightly to 95.67% for 7° mean rotation ($p < 2.2e^{-16}$). Additionally, maximum dose in the OARs and PTV again increases when plans are not reoptimized.

3.3 | Timings

We evaluate the computational effort on a AMD Ryzen 9 3950X CPU. While dose calculation and dose mapping is done in parallel threads, solving the linear optimization

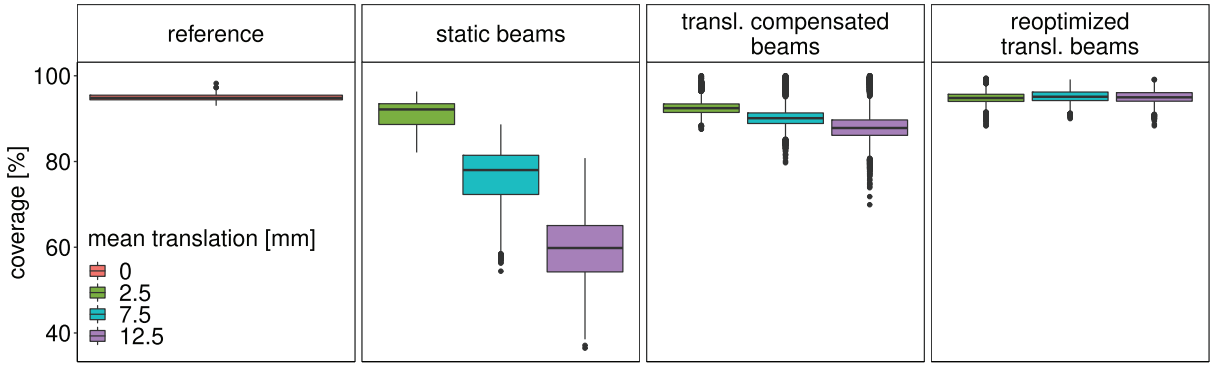

FIGURE 7 Boxplots of resulting coverage after a single target translation of different magnitudes during treatment. Shown are accumulated results for 50 patients. After translation delivery of 200 remaining beams is simulated with different compensation strategies.

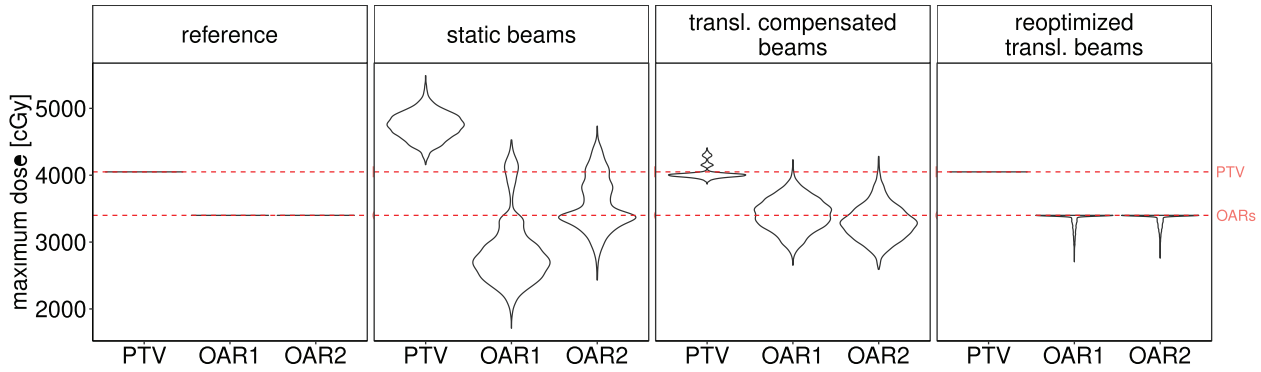

FIGURE 8 Violin plots of resulting maximum dose in respective VOIs after a single target translation with mean distance 12.5 mm. Note, that the maximum width is normalized, respectively. After translation delivery of 200 remaining beams is simulated with different compensation strategies. Shown in red is the prescribed maximum dose in PTV and OARs, respectively. OAR1: rectum, OAR2: bladder, PTV: prostate. OAR, organ at risk; PTV, planning target volume, VOIs, volumes of interest.

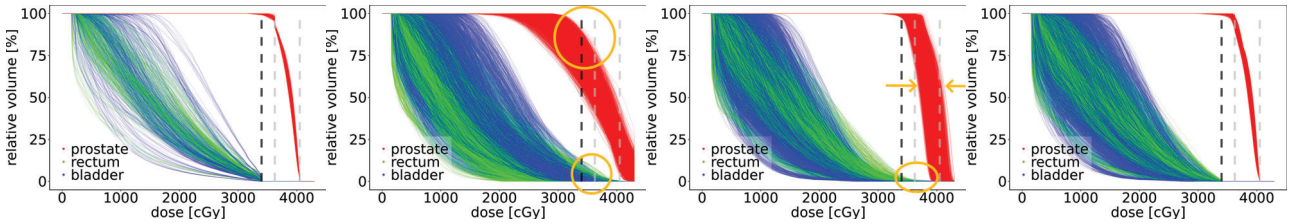

(a) reference (b) static beams (c) translated beams (d) reoptimized beams

FIGURE 9 DVHs of all cases for a static target (a), with target motion but static beams (b), with target motion and beam translation for compensation (c), and replanning after target and beam translation (d). Shown are results for 12.5 mm average target motion and no rotation. Gray dashed lines indicate prescribed dose and maximum PTV dose constraint; the black dashed line indicates maximum OAR dose constraints; orange circles and arrows highlight OAR overdosage, severe PTV underdosage, and PTV variation. OAR, organ at risk; PTV, planning target volume.

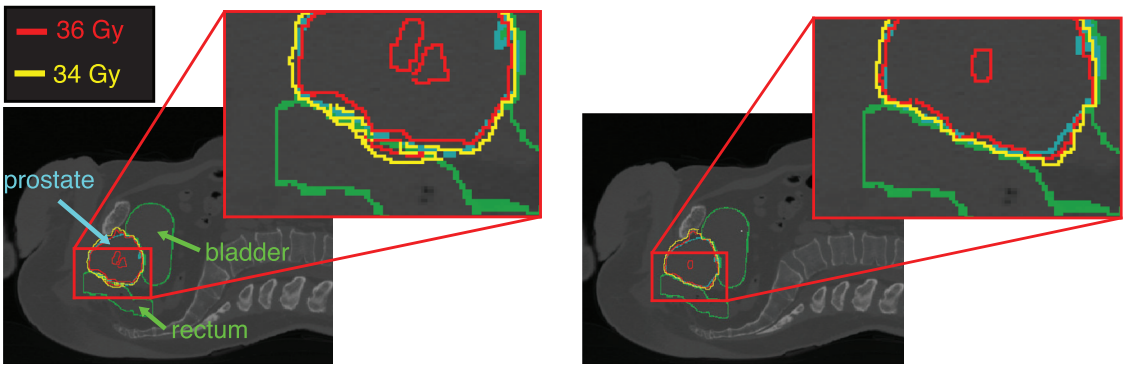

(a) motion compensated beams (b) reoptimized beams

FIGURE 10 Comparison of dose contours for motion compensated beams and reoptimized beams for one case. Shown are the prescribed dose to the PTV and the upper dose to the OARs. The resulting dose is transformed to the original geometry. Note, that the initial plan was partly delivered, contributing to the ill-defined dose gradient between PTV and OARs. OARs, organs at risk; PTV, planning target volume.

problem by the simplex based algorithm is sequential. Although, parallel approaches exist, the sequential simplex based optimizer had the best performance of the tested optimizers for this optimization problem and hardware.

Considering Figure 12, even when reoptimizing the weight of 200 beams, the complete runtime is below 6 s. In dose mapping, the time for setup of the optimization problem is included. The runtime increases for increasing number of reoptimized beams due to the increasing

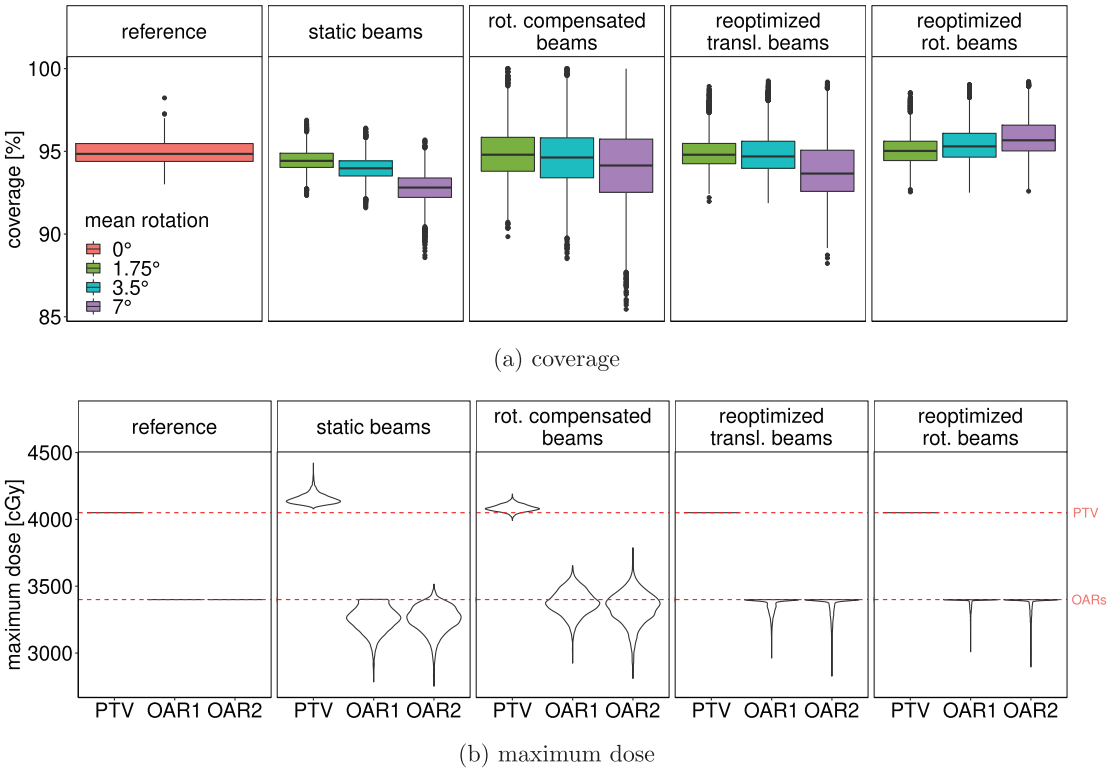

FIGURE 11 Boxplots of resulting coverage (a) and violin plots of maximum dose (b) after target rotation without translation. After rotation delivery of 200 remaining beams is simulated. The target is rotated randomly by angles sampled from normal distributions with different mean angles. Note that static beams result in the same dose distribution as translation compensated beams. The mean rotation for the maximum dose (b) is 7°.

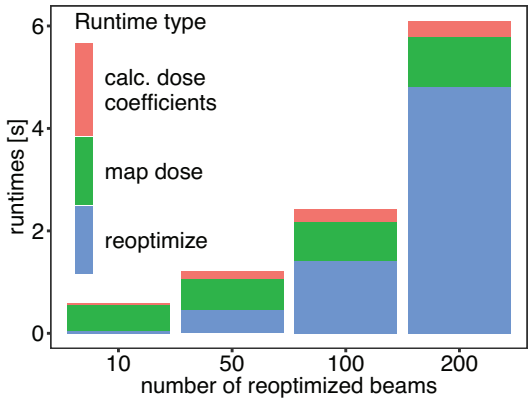

FIGURE 12 Average runtimes for dose coefficient calculation for remaining beams, for dose mapping and constraint adjustment of the moved VOIs, and for reoptimization. VOIs, volumes of interest.

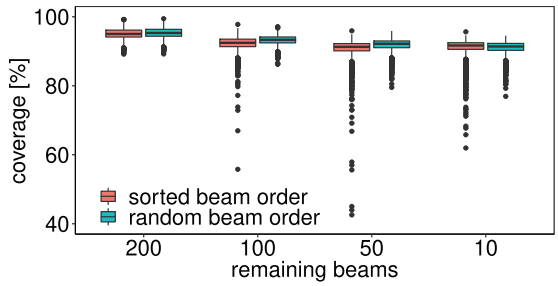

FIGURE 13 Boxplots of resulting coverage for replanning of translated and rotated beams after a random translation with a mean of 12.5 mm and a random rotation with a mean of 7° for a sorted beam delivery (a) and random order for beam delivery (b).

problem size, that is dose coefficients per voxel for each added beam as we established.

3.4 | Number of replanned beams

As Figure 13 shows, the coverage after reoptimization drops for most plans for decreasing number of reoptimized beams and large motion. Note however that upper constraints on the maximum dose are not exceeded. Figure 13 also shows the effect of the beam delivery order. Generally, randomized beam delivery results in more homogeneous dose delivery over time resulting in significantly ($p < 2.54e^{-6}$) higher coverage after reoptimization except for 10 remaining beams ($p = 0.055$).

4 | DISCUSSION

Considering Figure 7 and Figure 8, we have shown that intra-fractional replanning can compensate for the

coverage loss due to spontaneous target motion. In contrast to current adaption approaches including synchronous beam motion compensation, an increase in maximum OAR dose could be avoided. This is guaranteed by using a linear optimization problem for inverse planning.

When considering target rotation, non-reoptimized beams can lead to increased maximum dose in the PTV since the volume which has already received the prescribed dose can rotate into the focus of another beam. Note that this effect could occur even in perfectly spherical targets and not only irregularly shaped structures. While the shape of the prostate is more similar to a sphere than many other common treatment targets, rotation of the prostate can still reduce coverage without reoptimization if rotation is large as Figure 11 shows. Even when the beams follow the rotation, the radiological depth can change and thereby the induced dose. Reoptimization can compensate for this effect. Note that there is a tradeoff between homogeneity and coverage in the PTV which can be controlled by the constraints used during reoptimization. In contrast, this tradeoff cannot be controlled with conventional compensation by beam motion.

Intra-fractional reoptimization needs to be fast which we have shown even for a large number of reoptimized beams. Few previous works have studied intra-fractional replanning for conventional IMRT. Still, the computation time of our approach is well below the reported intra-fractional replanning time for IMRT by Kontaxis et al.[22]

While replanning generally increases coverage compared to translational compensation, Figure 9 shows that a decrease in plan quality can occur due to motion even after replanning. In particular, Figure 13 shows that average coverage decreases if target motion occurs toward the end of the treatment. When the majority of dose is delivered, feasible directions for additional dose delivery are few. Furthermore, when limited options to reweight the beams remain, the optimizer often cannot recover the original coverage of the reference plan.

Note that we only reweighted beams of the original treatment plan in this work. By resampling additional beams which were not included in the original plan, the decrease in coverage might be avoided. However, safety of these additional beams needs to be ensured without human supervision in an intra-fractional setting. Furthermore, optimizing the order of beam delivery for robustness could improve coverage, especially in case of motion at the final stages of the treatment. Note that this objective may compete with the treatment time when optimizing the order of beam delivery.

In this study we focus on simulated motion in the range of reported real motion.[12,28–30] Thereby, we avoid influence of segmentation inaccuracies and show proof of concept results for our approach. While the quality of automatic segmentation methods is often sufficient, further research is needed for intra-fractional use where limited manual correction is feasible. Furthermore, in-vivo motion is complex due to the interaction of tissue structures. It usually involves a combination of deformation, translation, and rotation. In particular OAR deformation can impact dose delivered to the OAR.[31] Still, deformation can be imaged intra-fractionally, for example, using fast volumetric US systems,[32] and with information about tissue deformation it is straight forward to apply our approach for deformation of PTV and OARs.

We estimate dose coefficients by virtually moving all voxels of the original VOI to the corresponding locations in the translated VOI. The CT is not deformed. While both the tissue property and physical path length influence the actual dose coefficients, the latter has been found to be of more importance for prostate radiation therapy.[33] Therefore, we assume this approach to be sufficiently accurate for our simulation study. Similarly, we move the delivered dose with the VOI to accumulate dose. Clinical motion data, for example, from US image guidance, could provide a more continuous basis for dose accumulation, for example, by dose warping.[34]

We simulate large motion and subsequent reoptimization once during treatment but slight target motion can also occur during the reoptimization time. However, small changes in geometry and periodic changes can generally be compensated well by synchronous beam motion. Therefore, this work focused on large deviations from the reference plan due to drift or sudden large motion. Since the time for reoptimization is short, our approach can be extended for reoptimization before delivery of every beam in future work.

5 | CONCLUSION

Intra-fractional reoptimization is a challenging task due to time constraints and limited human supervision. We apply linear optimization for fast constrained reoptimization after target motion. We simulate target translation and rotation during treatment and show that our approach improves coverage compared to the conventional intra-fractional adaption while retaining upper dose constraints. Average runtime of replanning is below 6 s making it promising for intra-fractional use.

ACKNOWLEDGMENTS

This work was partially funded by Deutsche Forschung sgemeinschaft (grants SCHL 1844/3-2 and SCHL 1844/6-1).

Open access funding enabled and organized by Projekt DEAL.

CONFLICT OF INTEREST STATEMENT

The authors declare that they have no conflict of interest.

INFORMED CONSENT

For this type of study informed consent is not required.

REFERENCES

1. Benedict SH, Galvin JM, Hinson W, et al. Stereotactic body radiation therapy: the report of AAPM Task Group 101. *Med Phys*. 2010;37:4078-4101.
2. D'Souza WD, Naqvi SA, Yu CX. Real-time intra-fraction-motion tracking using the treatment couch: a feasibility study. *Phys Med Biol*. 2005;50:4021-4033.
3. Sawant A, Venkat R, Srivastava V, et al. Management of three-dimensional intrafraction motion through real-time DMLC tracking. *Med Phys*. 2008;35:2050-2061.
4. Giraud P, Houle A. Respiratory gating for radiotherapy: main technical aspects and clinical benefits. *ISRN Pulmonol*. 2013;2013:1-13.
5. Kilby W, Naylor M, Dooley JR, Maurer CR, Sayeh S. 2 - A technical overview of the cyberknife system. In: Abedin-Nasab MH, eds. *Handbook of Robotic and Image-Guided Surgery*. Elsevier; 2020:15-38.
6. Colvill E, Booth J, Nill S, et al. A dosimetric comparison of real-time adaptive and non-adaptive radiotherapy: a multi-institutional study encompassing robotic, gimbaled, multileaf collimator and couch tracking. *Radiol Oncol*. 2016;119:159-165.
7. Schlaefer A, Fisseler J, Dieterich S, Shiomi H, Cleary K, Schweikard A. Feasibility of four-dimensional conformal planning for robotic radiosurgery. *Med Phys*. 2005;32:3786-3792.
8. Choi HS, Kang KM, Jeong BK, et al. Analysis of motion-dependent clinical outcome of tumor tracking stereotactic body radiotherapy for prostate cancer. *J Korean Med Sci*. 2018;33:e107.
9. Taillez A, Bimbai AM, Lacornerie T, Le Deley MC, Lartigau EF, Pasquier D. Studies of intra-fraction prostate motion during stereotactic irradiation in first irradiation and re-irradiation. *Front Oncol*. 2021;11:690422.
10. Hunt A, Hansen VN, Oelfke U, Nill S, Hafeez S. Adaptive radiotherapy enabled by MRI guidance. *Clin Oncol*. 2018;30:711-719.
11. Stanescu T, Shessel A, Carpino-Rocca C, et al. MRI-guided online adaptive stereotactic body radiation therapy of Liver and Pancreas Tumors on an MR-Linac system. *Cancers*. 2022;14:716.
12. McPartlin AJ, Li XA, Kershaw LE, et al. MRI-guided prostate adaptive radiotherapy - a systematic review. *Radiother Oncol*. 2016;119:371-380.
13. Byrne M, Archibald-Heeren B, Hu Y, et al. Varian ethos online adaptive radiotherapy for prostate cancer: early results of contouring accuracy, treatment plan quality, and treatment time. *J Appl Clin Med Phys*. 2022;23:e13479.
14. Ma T, Liu CW, Ahmed S, et al. Is adaptive planning necessary for patients with large tumor position displacements observed on daily image guidance during lung SBRT? *Med Dosim*. 2022;47:207-215.
15. Avgousti R, Antypas C, Armpilia C, et al. Adaptive radiation therapy: when, how and what are the benefits that literature provides? *Cancer Radiother*. 2022;26:622-636.
16. Men C, Jia X, Jiang SB. GPU-based ultra-fast direct aperture optimization for online adaptive radiation therapy. *Phys Med Biol*. 2010;55:4309-4319.
17. Wiersma RD, Liu X. A conceptual study on real-time adaptive radiation therapy optimization through ultra-fast beamlet control. *Biomed Phys Eng Express*. 2019;5:055016.
18. Antico M, Prinsen P, Cellini F, et al. Real-time adaptive planning method for radiotherapy treatment delivery for prostate cancer patients, based on a library of plans accounting for possible anatomy configuration changes. *PLoS ONE*. 2019;14:e0213002.
19. den Boer D, den Hartogh MD, Kotte ANTJ, et al. Comparison of Library of Plans with two daily adaptive strategies for whole bladder radiotherapy. *Phys Imaging Radiat Oncol*. 2021;20:82-87.
20. Katz AJ, Santoro M, Ashley R, Diblasio F, Witten M. Stereotactic body radiotherapy for organ-confined prostate cancer. *BMC Urology*. 2010;10:1.
21. Cahlon O, Hunt M, Zelefsky MJ. Intensity-modulated radiation therapy: supportive data for prostate cancer. *Semin Radiat Oncol*. 2008;18:48-57.
22. Kontaxis C, Bol GH, Stemkens B, et al. Towards fast online intrafraction replanning for free-breathing stereotactic body radiation therapy with the MR-linac. *Phys Med Biol*. 2017;62:7233-7248.
23. Kontaxis C, Bol GH, Lagendijk JJW, Raaymakers BW. A new methodology for inter- and intrafraction plan adaptation for the MR-linac. *Phys Med Biol*. 2015;60:7485-7497.
24. Kontaxis C, Bol GH, Lagendijk JJW, Raaymakers BW. Towards adaptive IMRT sequencing for the MR-linac. *Phys Med Biol*. 2015;60:2493-2509.
25. Mejnertsen L, Hewson E, Nguyen DT, Booth J, Keall P. Dose-based optimisation for multi-leaf collimator tracking during radiation therapy. *Phys Med Biol*. 2021;66:065027.
26. Schlaefer A, Schweikard A. Stepwise multi-criteria optimization for robotic radiosurgery. *Med Phys*. 2008;35:2094-2103.
27. Echner GG, Kilby W, Lee M, et al. The design, physical properties and clinical utility of an iris collimator for robotic radiosurgery. *Phys Med Biol*. 2009;54:5359-5380.
28. Ipsen S, Wulff D, Kuhlemann I, Schweikard A, Ernst F. Towards automated ultrasound imaging-robotic image acquisition in liver and prostate for long-term motion monitoring. *Phys Med Biol*. 2021;66:094002.
29. Ballhausen H, Kortmann E, Belka C, Li M. The promotion LMU dataset (2022 edition), prostate intra-fraction motion recorded by transperineal ultrasound. *Sci Data*. 2022;9:455.
30. Mah D, Freedman G, Milestone B, et al. Measurement of intrafractional prostate motion using magnetic resonance imaging. *Int J Radiat Oncol Biol Phys*. 2002;54:568-575.
31. Dang J, Li W, Navarro I, et al. Impact of intrafraction changes in delivered dose of the day for prostate cancer patients treated with stereotactic body radiotherapy via MR-Linac. *Tech Innov Patient Support Radiat Oncol*. 2022.
32. Baumann M, Mozer P, Daanen V, Troccaz J. Prostate biopsy tracking with deformation estimation. *Med Image Anal*. 2012;16:562-576.
33. Kerkhof EM, Balter JM, Vineberg K, Raaymakers BW. Treatment plan adaptation for MRI-guided radiotherapy using solely MRI data: a CT-based simulation study. *Phys Med Biol*. 2010;55:N433-40.
34. Chetty IJ, Rosu-Bubulac M. Deformable registration for dose accumulation. *Semin Radiat Oncol*. 2019;29:198-208.

How to cite this article: Gerlach S, Hofmann T, Fürweger C, Schlaefer A. Towards fast adaptive replanning by constrained reoptimization for intra-fractional non-periodic motion during robotic SBRT. *Med Phys*. 2023;1-10. https://doi.org/10.1002/mp.16381